CHINESE JOURNAL OF PHYSICS VOL. 49 , NO. 1 FEBRUARY 2011

Nature of the Phonon Beam emitted by the Ruby Saser

L. G. Tilstra,[1] A. F. M. Arts,[1] and H. W. de Wijn[1,*]

[1] *Debye Institute, Utrecht University, Utrecht, The Netherlands*

(Received April 8, 2010)

The properties of the phonon beam emitted by the optically pumped "hot zone" in the ruby saser are examined. The phonons generated are detected via the R_1 luminescence and analyzed by the use of coherent Bloch-type equations. The phonons are found to reach occupations p of order 3000, which at the relevant phonon frequency of 50.4 GHz corresponds to temperatures of order 5000 K. The spectral and angular distributions of the beam have been measured in experiments involving pumped zones at either end of the crystal, one serving as generator, the other one as detector. The spectral distribution is 54 ± 10 MHz wide at half value, or 0.1% of the phonon frequency. Within errors, this is in conformity with the inhomogeneous Gaussian frequency spread inherent to the sasering one-phonon transition. The angular divergence appears to be governed by the geometry of the hot zone. Under the prevailing conditions it measures 3 degrees of arc to either side.

PACS numbers: 63.20.-e

I. INTRODUCTION

The last decade has seen the realization of the acoustic analogue of the laser, which presently is referred to by the acronym saser (sound amplification through stimulated emission of acoustic radiation). The first condition required for a saser is the presence of a "hot" zone, an ensemble of two-level quantum systems pumped into their upper level and connected by a one-phonon transition. While at this point stimulated emission of phonons is quite common, a genuine saser additionally requires the generated phonons to propagate in a collimated beam. This beam preferably is to pass repetitively through the inverted zone to engage in further amplification upon each passage. Dilute optically excited ruby may act as a saser [1–3]. In this paper, we discuss the properties of the phonon beam, in particular the phonon occupation reached, its spectral width, and its angular divergence.

II. RUBY SASER

The principle of the ruby saser is depicted in Fig. 1(a). The "hot" zone, of limited length β, is formed by Cr^{3+} ions residing in the upper state E_+ of the long-lived Zeeman-split $\overline{E}(^2E)$ metastable doublet (radiative lifetime $\tau_R \approx 4$ ms). Its population is achieved by selective pulsed optical pumping, after which an avalanche of resonant phonons occurs. In the experiments, the population density N_- of the E_- level, i.e., number of phonons generated, is recorded at any time via the intensity of the $E_- \rightarrow {}^4A_2, M_s = +1/2$ com-

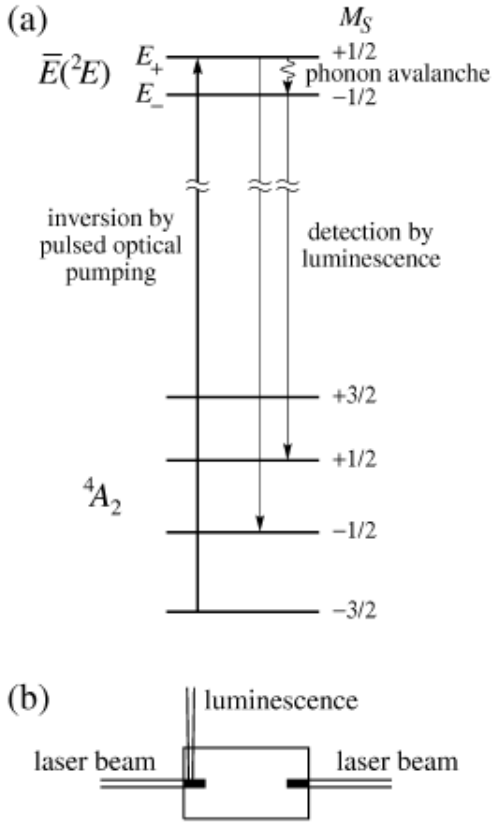

FIG. 1: (a) The relevant Zeeman-split level scheme of Cr^{3+} in ruby. Pulsed optical pumping leaves the populations of the $\overline{E}(^2E)$ doublet inverted. The ensuing phonon avalanche is detected via the R_1 luminescence. (b) The two-zone experiment. Phonon generation is at the right end, detection by luminescence at the left.

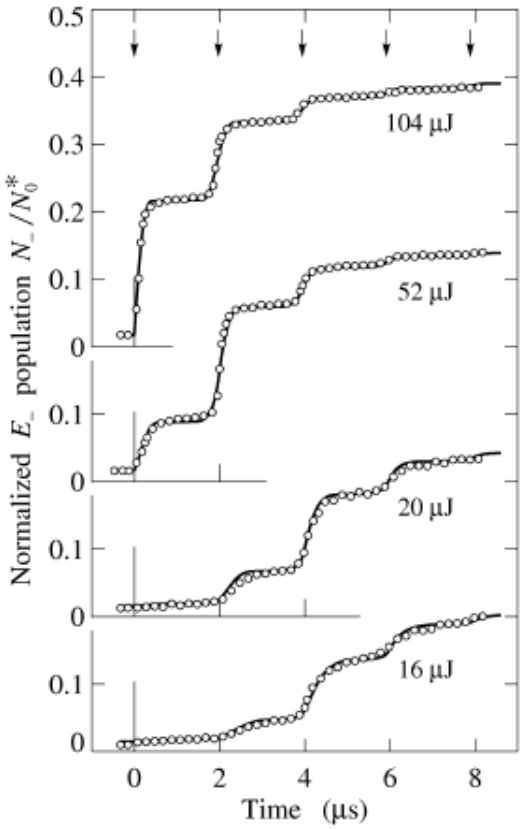

FIG. 2: Normalized population N_-/N_0^* of the lower doublet level, which is a direct measure of the number of phonons generated, versus the time after inversion of the $\overline{E}(^2E)$ doublet. The labels denote the pulse energy of the exciting laser. Arrows mark the successive passages through the hot zone at intervals $2L/v$.

ponent of the R_1 luminescence. Note that direct comparison with the Kramers-conjugate $E_+ \rightarrow {}^4A_2, M_s = -1/2$ luminescent intensity [cf. Fig. 1(a)] allows us to express N_- in relation to the initial population per unit volume N_0^*.

The sample, a cuboidal Czochralski-grown single crystal, has a Cr^{3+} concentration of 500 at.ppm, or 1.2×10^{25} m^{-3}. It measures $6.60 \times 4.63 \times 1.91$ mm^3, the crystalline a axis being parallel to the longest edges. The surface roughness is of order 10 nm, substantially smaller than the 135-nm phonon wavelength. As to the experimental conditions [3], the ruby crystal was mounted in a split-coil superconducting magnet, supplying a field of 3.48 T oriented at 65° from the c axis, to separate the $\overline{E}(^2E)$ states by $\omega/2\pi c = 1.68$ cm^{-1}, or $\nu = \omega/2\pi = 50.4$ GHz. Cooling down to 1.4 K eliminated any direct and Orbach thermal

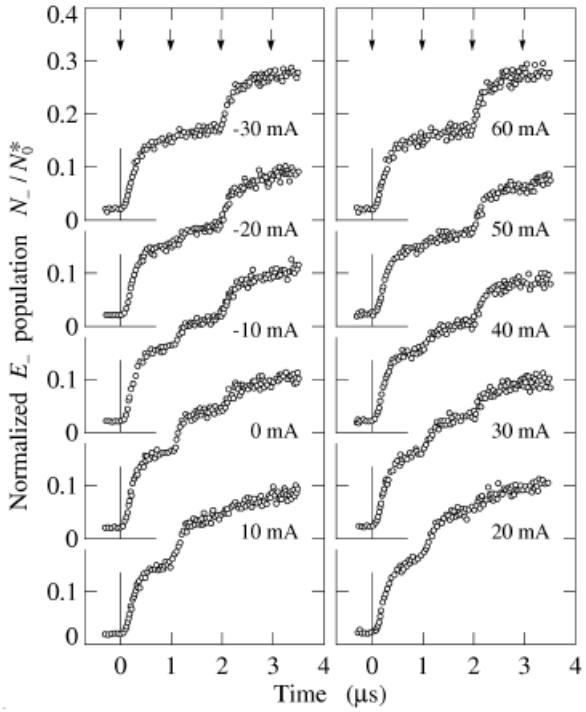

FIG. 3: Normalized population N_-/N_0^* of the lower doublet level, i.e., the normalized number of phonons generated, versus the time following population inversion. The traces are derived from the luminescent intensities for various frequency shifts of the generation zone relative to the detection zone. The labels denote the currents through the solenoid invoking the frequency-shifting magnetic field gradient, with 10 mA corresponding to a frequency shift of 14.3 MHz. The arrows mark the passages of phonons through the detection zone at intervals L/v.

relaxation within $\overline{E}(^2E)$, and ensured virtually unhindered ballistic travel of the phonons through the crystal. The optical pumping into E_+ was achieved with a dye laser delivering light pulses of 8-ns duration at 50 Hz. The laser beam, whose central portion was focused to a waist 200 μm in diameter, was incident along the a axis. The beam was polarized for maximum optical absorption, to create an excited zone $\beta = 1.5 \pm 0.2$ mm in length. The R_1 luminescence was resolved with a 0.85-m double monochromator followed by standard photon-counting techniques.

Figure 2 presents experimental traces of N_-/N_0^*, as measured with a single excited zone versus the time for a series of pulse energies of the exciting laser. These traces, which feature steps at intervals $L/v = 1.97$ μs, i.e., the time needed for T_1 phonons to complete a round trip through the crystal with velocity $v = 6.7$ km/s. The initial rise marks the phonons released by stimulated emission immediately following the laser pulse, while the next steps signify the further rise of the phonon density during the successive passages of the phonon beam through the inverted zone after completion of a round trip.

III. PHONON OCCUPATION

To calculate the phonon density in a coherent description, we set up a set of equations of motion for the amplitude $U(x,t)$ of the traveling acoustic wave, while it is coupled, with coupling constant γ, to the combined transverse component $S^x(x,t)$ of the Cr^{3+} spins. We decompose $U(x,t)$ into right- and left-traveling waves with amplitude envelopes U_R and U_L. Similarly, we introduce right- and left-going components S_R and S_L of the transverse spin density $2N^*S^x(x,t)$, where the $\overline{E}(^2E)$ population density N^* expresses that only part of the Al sites are occupied by excited Cr^{3+}. While $U(x,t)$ and $S^x(x,t)$ are coupled directly, they in higher order also affect the longitudinal spin density $2N^*S^z(x,t)$, which is equal to the difference $n = N_+ - N_-$ of the $\overline{E}(^2E)$ population densities. The Bloch-type equations of motion for U_R, U_L, S_R, S_L, and n, which all vary slowly over the length of the crystal, then read [2]

$$\begin{aligned}
&\partial U_R/\partial t + v(\partial U_R/\partial x) = -(a^4\gamma\hbar/2Mv)S_R, \quad \partial S_R/\partial t = -a\gamma k U_R n - S_R/T_2,\\
&\partial U_L/\partial t - v(\partial U_L/\partial x) = +(a^4\gamma\hbar/2Mv)S_L, \quad \partial S_L/\partial t = +a\gamma k U_L n - S_L/T_2,\\
&\partial n/\partial t = 2a\gamma k(U_R^*S_R + U_R S_R^* - U_L^*S_L - U_L S_L^*) - [(1+2p_0)n + N^*]/T_1.
\end{aligned} \tag{1}$$

Here, $k = \omega/v$ is the acoustic wave vector, $a \approx 0.5$ nm is the lattice constant, and $M = 3.39 \times 10^{-25}$ kg is the mass of the unit cell containing two Al_2O_3. The coupled Eqs. (1) include thermal relaxation and spin dephasing within $\overline{E}(^2E)$ in the customary heuristic way. Under the present conditions, $T_1 = 0.67$ ms, $p_0 = 0.22$, and $T_2 \approx 7$ ns [2]. A reasonable estimate for γ, which measures the spin-lattice coupling, may be derived from T_1 and the system parameters [3]. The model is completed by accounting for phonon loss at the crystal boundaries by multiplying U_R and U_L upon reflection by an overall reflectance $R < 1$, i.e., $U_L = -RU_R$ at the right end, and similarly at the left end. For start-up of the phonon avalanche, the Bloch equations further require small, but finite, initial wave amplitudes, which are of no concern once the avalanche has overcome the threshold.

The analysis of the traces in Fig. 2 proceeds by numerical simulation of Eqs. (1) and subsequent fitting of the initial population N_0^* and the reflectance R to the traces. Here, the appropriate spatial profile of the initial inversion density is inserted, while the length of the crystal is subdivided into 200 sections. The resultant wave amplitudes $2|U_R|$ and $2|U_L|$ reach values up to 80 fm after a few passages. To convert these amplitudes to phonon occupation numbers p, one usually equates the energy content $2NM\omega^2|U|^2$ of the corresponding classical harmonic lattice oscillator to the phonon-mode energy $\hbar\omega(p+\frac{1}{2})$ summed over the participating phonon modes. That is,

$$|U|^2 = \frac{\hbar\omega(p+\frac{1}{2})}{2NM\omega^2}\rho\Delta\nu \tag{2}$$

in which $N = 1.2 \times 10^{28}$ m^{-3} is the number of unit cells per unit volume, ρ is the density of phonon modes per unit frequency, and $\Delta\nu$ is the line width (see below). In the Debye approximation, $\rho\Delta\nu = 1.3 \times 10^{19}$ m^{-3} for the two acoustic T_1 branches combined. Equation (2) then yields estimates for p as high as 3000, to be compared to $p_0 = 1/[\exp(\hbar\omega/k_BT) -$

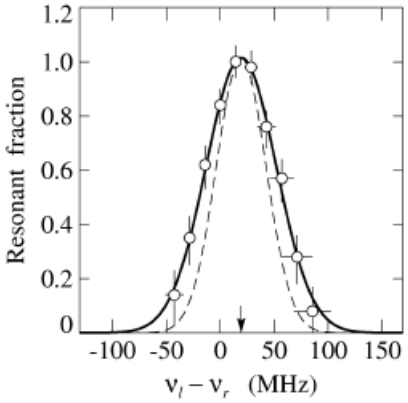

FIG. 4: Fraction of the phonon beam leaving the generation zone that is resonant with Cr^3+ in the detection zone versus the frequency shift. The full curve is a fitted Gaussian. The dashed curve is the frequency spread remaining after deconvolution for the detector. The arrow indicates the constant residual shift due to the main magnet.

1] = 0.22 for thermal excitation alone. At the relevant frequency, these p correspond to phonon "temperatures" of order $\hbar\omega/k_B \approx 5000$ K.

Another estimate of p may be derived from the rise of the population in the lower $\overline{E}(^2E)$ level. This rise, when interpreted in terms of rate equations for the $\overline{E}(^2E)$ populations $N_\pm$ and the phonon occupation p, grows with time constant $T_1^* = T_1/(1+p) \approx 0.2\ \mu$s, compared to $T_1 = 0.67$ ms for spontaneous emission only. This again yields $p \approx 3000$. This is the more remarkable because these rate equations, unlike Eqs. (1), provide an *incoherent* description, and therefore are essentially deficient.

IV. FREQUENCY DISTRIBUTION

To study the spectral width and, in Sec. V below, the angular divergence of the acoustic wave, we introduce a second optically excited zone at the opposite end of the crystal. In the new zone, at the right in Fig. 1(b), an additional phonon beam is generated, which, after crossing the crystal, may be examined in the original zone at the left remaining to serve as luminescent detector. In particular, the two-zone arrangement allows us to measure the spectral distribution of the beam with the help of a small magnetic gradient field mutually shifting the center frequencies of the two zones. The gradient field is supplied by an oppositely wound split-coil superconducting minimagnet located in the sample area.

The measured traces of N_-/N_0^* versus the time are displayed in Fig. 3 for various frequency displacements $\nu_l - \nu_r$ of the zones. The stepwise rise of N_- now occurs at intervals L/v, in lieu of $2L/v$. The even steps arise, as in Sec. II, from the avalanche in the left zone and the phonons native to this zone upon their return, while the odd steps arise from the passage and further amplification of phonons originating from the right zone.

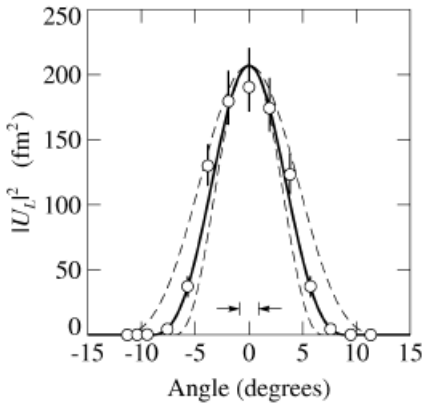

FIG. 5: Squared half amplitude $|U_L|^2$ versus the angle of the trajectory from the generation zone to the detection zone. The solid line corresponds to a model calculation for a generation zone of 200 μm diameter, while the dashed lines refer to diameters of 100 and 300 μm. The detection zone subtends a viewing angle of 1.8 degrees of arc, as indicated by arrows.

To derive which fraction of the latter phonons are resonant with the left zone, we again rely on simulations of Eqs. (1), but with the new zone included. The results are shown as data points in Fig. 4, where the horizontal error bars originate mainly from converting minimagnet currents to frequencies. A Gaussian line shape with a full width of 77 ± 15 MHz at half maximum nicely tracks the data points (full curve in Fig. 4), the offset of 19 ± 5 MHz being due to residual inhomogeneity of the static magnetic field. It is quite reasonable to assume that the frequency distributions of the two zones are equal. For the phonon beam traveling through the crystal, self-deconvolution then leaves a Gaussian with a full width at half maximum of 54 ± 10 MHz (dashed curve in Fig. 4), only 0.1% of the phonon frequency.

This result compares with the width of the $\overline{E}(^2E)$ line as measured in archetypal optically detected EPR experiments [5, 6]. The line is known to be inhomogeneously broadened, i.e., to be made up of packets of distinct frequencies. Sources contributing to inhomogeneous broadening of the $\overline{E}(^2E)$ transition are random magnetic fields from Al nuclear moments near excited Cr^{3+} and wandering of the c axis by lattice imperfections, both sources favoring a Gaussian profile. Note also in this context that the time $T_2 \approx 7$ ns characterizing dephasing of the transverse spin components [2] compares, within errors, with the time $1/\pi\Delta\nu = 6$ ns associated with the inhomogeneous width. The homogeneous component of the line width amounts to $(1 + 2p)/\pi T_1$. It is severely enhanced, but does not exceed 1 MHz even at the phonon occupations reached ($p \approx 3000$). The conclusion is therefore justified that the phonon avalanche and the associated acoustic wave are inhomogeneously broadened along with the one-phonon transition, yet that each packet maintains a sizable degree of coherence over longer times. It is likely that these individual packets narrow with increasing stimulated emission, but observing this would require a coherent technique [7].

V. ANGULAR DISTRIBUTION

In a similar two-zone experiment, featuring lateral displacements of the generation zone while leaving the frequency fixed, we measure the angular dependence of the phonon beam. Again simulations based on Eqs. (1) are necessary to find the wave amplitudes. Differently from above, however, the analysis cannot be extended to times beyond a single crossing through the crystal, because at larger angles the phonon beam may miss the detection zone altogether upon its next arrival. The results for $|U_L|^2$ after the first crossing are, for moderate optical pulse energies, displayed in Fig. 5. The measured profile has a width of about 8 degrees of arc. Deconvolution for the finite resolution of the detection zone, which subtends an angle of 1.8 degrees as seen from the generating zone, leaves a divergence of 3 degrees of arc to either side.

We finally calculate the divergence of the acoustic beam from the geometry of the generation zone. At the start of an avalanche, phonons spontaneously emitted by optically excited Cr^{3+} release further phonons by iterative stimulated emission. Stimulated emission, however, compels the added phonons to travel along the direction first chosen [8], to form a "ray" of coherent phonons. According to Eqs. (1), these rays grow exponentially in intensity with the distance traveled times the local $N^*(x, y, z)$, until phonon occupations of order 10^3 are reached. Rays thus contribute significantly only if they traverse the zone over most of its length. In the numerical calculations of this model, we let some 10^6 rays depart in all directions from, evenly distributed, the far end of the generation zone. These rays are subsequently amplified according to Eqs. (1), and their contributions to $|U_L|^2$ collected in a square matrix of finite bins at the other end of the crystal. The matrix is finally read out by a circular detector of appropriate diameter scanning across this matrix, to find $|U_L|^2$ integrated over the detector area as a function of the angle connecting the generation and detection zones. Fair agreement is obtained for realistic values of the parameters specifying the geometry of the generation zone as well as the acceptance area of the detection zone, viz., $\beta = 1.5$ mm and $d = 200$ μm (full curve in Fig. 5). For comparison, computed results for $d = 100$ and 300 μm are also shown (dashed lines). These results lead to the conclusion that the divergence of the acoustic wave is governed by the geometry of the hot zone.

References

* Electronic address: h.w.dewijn@uu.nl

[1] L. G. Tilstra, A. F. M. Arts, and H. W. de Wijn, J. Lumin. **94–95**, 751 (2001).
[2] L. G. Tilstra, A. F. M. Arts, and H. W. de Wijn, Phys. Rev. B **68**, 144302 (2003).
[3] L. G. Tilstra, A. F. M. Arts, and H. W. de Wijn, Phys. Rev. B **76**, 024302 (2007).
[4] C. Leonardi, J. C. MacGillivray, S. Libermans, and M. S. Feld, Phys. Rev. B **11**, 3298 (1973).
[5] S. Geschwind, G. E. Devlin, R. L. Cohen, and S. R. Chinn, Phys. Rev. **137**, A1087 (1965).
[6] T. Muramoto, J. Phys. Soc. Japan **35**, 921 (1973).
[7] R. P. Beardsley, A. V. Akimov, M. Henini, and A. J. Kent, Phys. Rev. Lett. **104**, 085501 (2010).
[8] M. O. Scully and M. S. Zubairy, *Quantum Optics* (Cambridge Univ. Press, 1997).